


Merging Bound States in the Continuum at Off-High Symmetry Points

Meng Kang,¹ Shunping Zhang,^{1,*} Meng Xiao^{1,†}, and Hongxing Xu^{1,2,‡}

¹*School of Physics and Technology, Center for Nanoscience and Nanotechnology, and Key Laboratory of Artificial Micro- and Nano-structures of Ministry of Education, Wuhan University, Wuhan 430072, China*

²*The Institute for Advanced Studies, Wuhan University, Wuhan 430072, China*

 (Received 5 October 2020; accepted 15 February 2021; published 19 March 2021)

Bound states in the continuum (BICs) confine resonances embedded in a continuous spectrum by eliminating radiation loss. Merging multiple BICs provides a promising approach to further reduce the scattering losses caused by fabrication imperfections. However, to date, BIC merging has been limited to only the Γ point, which constrains potential application scenarios such as beam steering and directional vector beams. Here, we propose a new scheme to construct merging BICs at almost an arbitrary point in reciprocal space. Our approach utilizes the topological features of BICs on photonic crystal slabs, and we merge a Friedrich-Wintgen BIC and an accidental BIC. The Q factors of the resulting merging BIC are enhanced for a broad wave vector range compared with both the original Friedrich-Wintgen BIC and the accidental BIC. Since Friedrich-Wintgen BICs and accidental BICs are quite common in the band structure, our proposal provides a general approach to realize off- Γ merging BICs with superhigh Q factors that can substantially enhance nonlinear and quantum effects and boost the performance of on-chip photonic devices.

DOI: [10.1103/PhysRevLett.126.117402](https://doi.org/10.1103/PhysRevLett.126.117402)

Bound states in the continuum (BICs) are localized states with infinite lifetimes even in the presence of a continuous spectrum with matched energy and momentum [1]. Though initially proposed as a mathematical curiosity in quantum mechanics [2], BICs have attracted extensive attention in both quantum and classical waves [3–20]. To date, various mechanisms have been proposed to construct BICs through symmetry mismatch [9–11,19], parameter tuning [3,12,13,16,18,21], environment engineering [20], topological charge evolution [22,23], anisotropy utilization [17], and parity-time symmetry [24]. Their unique features in confining waves lead to miscellaneous applications requiring large-area field enhancement [25–38].

In photonic crystal slabs (PCSs), in addition to the well-known symmetry-protected BICs [11,39] (usually fixed at high symmetric points), accidental BICs [12], whose topological nature has been revealed recently [40–43], exist. The topological nature of BICs ensures that BICs can be continuously moved in reciprocal space as we vary the structure while keeping the symmetry of the system unchanged [40]. Thus, one can tune multiple BICs to the same wave vector to form a merging BIC [44]. In practical on-chip resonators, the Q factor of an isolated BIC is fundamentally limited by inevitable fabrication imperfections that couple BICs with nearby radiative states. Merging BICs can further suppress the radiation loss of nearby states compared with isolated BICs, which provides a promising approach to overcome the scattering losses caused by fabrication imperfections or disorders [44]. However, to date, merging BICs on PCSs has been limited

to the Brillouin zone center (Γ) only. On the other hand, many potential applications of BICs on PCS desire momentum selection, i.e., cannot be realized with (merging) BICs at Γ . These applications include but are not limited to beam steering [34,45], directional vector beams [46–48], diffraction-free beams [49], optical fibers [50,51], narrowband filters [52], modulators [53], and sensors [54] based on angular selectivity. Thus, merging BICs at arbitrary k points is of significant importance for numerous k -dependent applications, as their ultrahigh Q factors are robust against fabrication imperfections.

In this Letter, we propose a new mechanism that enables the construction of merging BICs at almost an arbitrary position in reciprocal space. To be more specific, we merge one Friedrich-Wintgen BIC (FW-BIC) [3] with another accidental BIC with opposite topological charges. As the location of the FW-BIC is weakly bound to the anticrossing point of two modes, which in general can be moved, the merging BIC we construct is thus no longer fixed to high symmetry points. We also design a PCS made of Si_3N_4 and immersed in a liquid (common in the laboratory) to demonstrate our idea, which can be readily verified experimentally. The merging BIC can be shifted to a general position as we further reduce the symmetry of PCSs.

The red line in Fig. 1(a) sketches two isolated BICs whose locations can be changed. One can force two BICs with opposite topological charges to merge [blue line in Fig. 1(a)] by suitably varying the structure parameters. The merging state is a topologically enabled BIC, i.e., a merging BIC, with an infinite Q factor at the BIC and

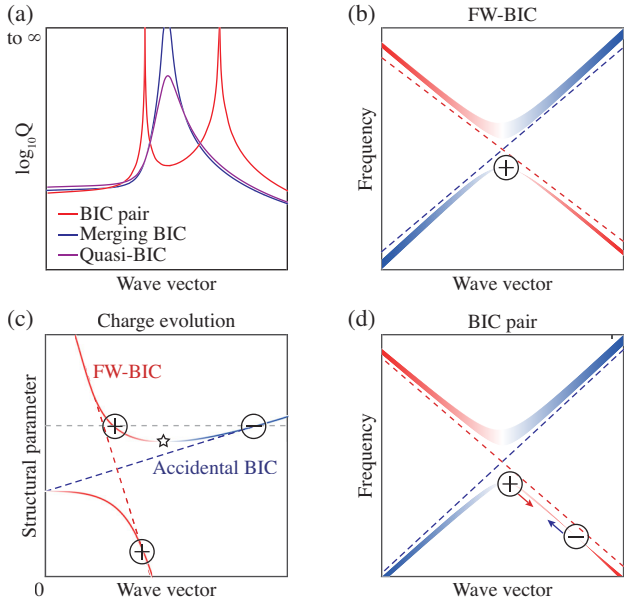


FIG. 1. (a) Sketch of the Q factor distribution for the BIC pair (red), merging BIC (cyan), and quasi-BIC (magenta). (b) Anti-crossing of two coupled resonances induces an FW-BIC with a positive topological charge. (c) Charge evolution of a FW-BIC with a positive topological charge and an accidental BIC with a negative topological charge as we vary the structural parameter. The gray dashed line denotes the case with a BIC pair, and this BIC pair merges at the position marked by the star and subsequently annihilates. The trajectories of charges show the feature of anticrossing, where the red and blue dashed lines are just for eye guidance. (d) The presence of an accidental BIC (assumed to exhibit a negative topological charge) close to the anticrossing point. The FW-BIC and the accidental BIC move towards each other as we tune the structure parameter. In (b) and (d), the line thickness represents the decay rate, and the color illustrates the hybridization of the two modes. Dashed lines indicate the dispersions of the two modes without interaction.

enhanced Q factors for states nearby compared with the original two isolated BICs. When the structure parameters are further tuned, the two isolated BICs with opposite charges annihilate with each other and form a quasi-BIC as a supercavity [55] with the Q factor reaching a high maximum value [purple curve in Fig. 1(a)]. In our case, one of the two BICs is an accidental BIC, as in Refs. [12,40], and the other is an FW-BIC.

Friedrich-Wintgen BIC.—The FW-BIC [3] is a special type of BIC obtained through parameter tuning. Unlike accidental BICs that need only one single resonance, a FW-BIC is formed by tuning the interaction between two (or among more) resonances. As sketched in Fig. 1(b), we consider two modes with resonance frequencies ω_1 and ω_2 (red and blue dashed lines) and different decay rates γ_1 and γ_2 , respectively. Without coupling, they cross each other as functions of the wave vector. If they couple through the same radiation channel, according to temporal coupled-mode theory [56], the Hamiltonian can be written as follows [3,57,59].

$$H = \begin{bmatrix} \omega_1 & \kappa \\ \kappa & \omega_2 \end{bmatrix} - i \begin{bmatrix} \gamma_1 & \sqrt{\gamma_1\gamma_2} \exp(i\psi) \\ \sqrt{\gamma_1\gamma_2} \exp(-i\psi) & \gamma_2 \end{bmatrix}, \quad (1)$$

where κ and $\sqrt{\gamma_1\gamma_2} \exp(i\psi)$ are the near-field and radiation coupling, respectively. Here ψ is the phase shift of radiation interference between the two resonances, which can be made 0 or π through parameter tuning or forced by symmetry [57]. With coupling, they hybridize as sketched in Fig. 1(b) with the colored strips, where the color indicates the component, and the width of strips represents the decay rate. Near the anticrossing point, one mode becomes lossier and the other mode becomes lossless, i.e., reaching the BIC condition, when

$$\kappa(\gamma_1 - \gamma_2)e^{-i\psi} = \sqrt{\gamma_1\gamma_2}(\omega_1 - \omega_2). \quad (2)$$

Thus, when $\kappa = 0$ or $\gamma_1 = \gamma_2$, a BIC is obtained when $\omega_1 = \omega_2$. In a more general case, $\kappa \approx 0$ and $\gamma_1 \approx \gamma_2$, and then the FW-BIC is weakly bound to the anticrossing point, as denoted by the black circle in Fig. 1(b). When $\text{sgn}(\kappa e^{-i\psi}) > 0$, the FW-BIC appears on the lower band; otherwise, it appears on the upper band. Here, for illustration, the FW-BIC is assumed on the lower band and exhibits topological charge +1.

Merging BIC mechanism.—When we vary the structural parameter, the position of the anticrossing point gradually shifts [red dashed line in Fig. 1(c)], and hence the FW-BIC bound to it [red solid curve in Fig. 1(c)] shifts as well. We further assume that there is another accidental BIC possessing the opposite charge and on the lower band, whose location also changes as the structural parameter varying [blue dashed line in Fig. 1(c)]. In other words, the variance in structural parameters brings an accidental BIC close to the FW-BIC from the wave vector far away. At the dashed gray line in Fig. 1(c), a BIC pair consisting of one FW-BIC and one accidental BIC coexist. Figure 1(d) sketches the corresponding band structure; therein, the accidental BIC is located in the lower right corner. As we change the structural parameter downward from the gray dashed line in Fig. 1(c), these two isolated BICs gradually approach each other and finally merge at the position marked by the star in Fig. 1(c). Thus we generate a merging BIC at off-high symmetry points. Moreover, if we continue to change the structural parameter, the FW-BIC and accidental BIC are annihilated to produce a quasi-BIC; thus, no FW-BIC persists.

Photonic crystal slab exhibiting an off- Γ merging BIC.—We now numerically investigate a PCS that fits the mechanism we discussed above using COMSOL Multiphysics software based on the finite-element method [60] (Supplemental Material [57], Sec. I). Our system consists of a Si_3N_4 PCS immersed in a liquid ($n = 1.46$, common in the laboratory) and etched with a square lattice of cylindrical holes [Fig. 2(a)]. The typical band structure of our PCS is shown in Fig. 2(b). Our system exhibits $\{C_{4v}, \sigma_h, T\}$ symmetries, and all the modes can be classified as TE -like

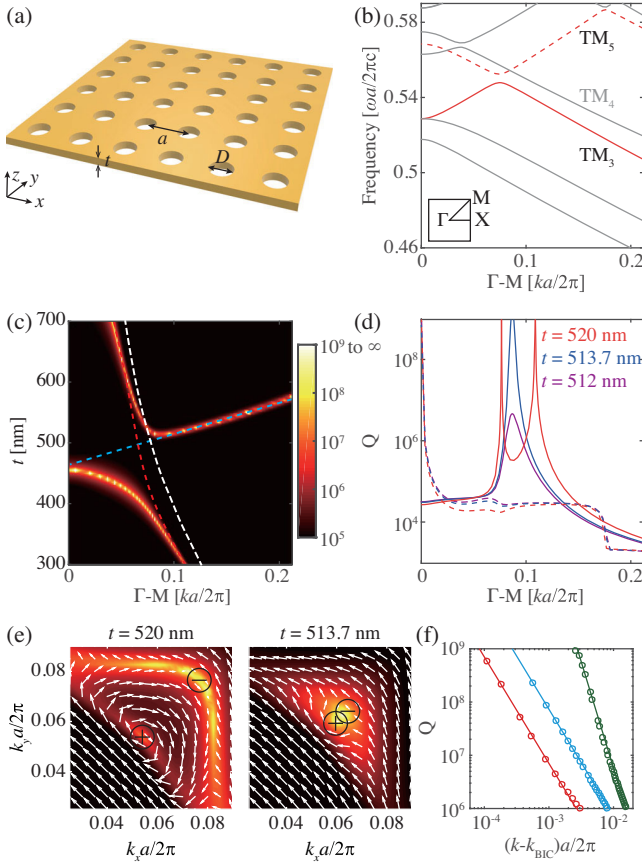


FIG. 2. (a) Diagram of the Si_3N_4 (refractive index $n = 2.02$) PCS with circular holes etched. The PCS is immersed in a liquid with refractive index $n = 1.46$. The lattice constant is $a = 334$ nm, and the diameter of the hole is $D = 160$ nm. (b) Simulated TM -like band structures at $t = 520$ nm. Here, the TM_3 and TM_5 bands anticross with each other. (c) Simulated quality factor Q evolution for the TM_3 band along the ΓM direction as we vary t . The bright curves show the trajectories of BICs. (d) Q factor distribution along the ΓM direction for the TM_3 (solid lines) and TM_5 (dashed lines) bands for various thicknesses. (e) Calculated polarization vectors around BICs with the Q factor as background in the Brillouin zone for $t = 520$ and $t = 513.7$ nm. (f) Open circles represent the Q factors as functions of the wave vector away from the BICs along the ΓM direction, where red is for the FW-BIC, cyan is for the accidental BIC at $t = 520$ nm, and green is for the merging BIC at $t = 513.7$ nm. The lines represent the corresponding fitting curves with $(k - k_{\text{BIC}})^{-2}$ (red and cyan) and $(k - k_{\text{BIC}})^{-4}$ (green).

or TM -like. Here, we show only the TM -like modes and label the band according to their frequency at Γ . Mode anticrossing features are actually quite common on the band structure. The red solid line (TM_3) and dashed line (TM_5) highlight two such modes that anticross each other along the ΓM direction at $ka = 0.15\pi$. These two bands reside in the region with only two radiation channels, i.e., the zero diffraction order with S and P polarizations. As the P polarization radiation channel here is forbidden by the mirror symmetry along the ΓM direction (σ_d), the

anticrossing of bands TM_3 and TM_5 fits in the Hamiltonian in Eq. (1) (Supplemental Material [57], Sec. II). Note here that bands TM_5 and TM_4 cross as they belong to different representations of σ_d (Supplemental Material [57], Sec. II).

Now, we focus on the anticrossing point of bands TM_3 and TM_5 and gradually vary the thickness of the Si_3N_4 PCS (t). The anticrossing point is quite stable when we vary t [the white dashed line in Fig. 2(c)]. We also plot the Q factor of the TM_3 band along the ΓM direction as a function of t . Here, two bright curves indicate very high Q factors that are tracks of BICs. For confirmation, we provide the Q factors along ΓM for $t = 520$ nm in Fig. 2(d) with the solid red line; therein, two isolated BICs are clear. Since our system exhibits the same symmetries as Ref. [40], these two isolated BICs possess nonzero topological charges. The left panel of Fig. 2(e) gives the polarization vectors together with the Q factor as the background of the TM_3 band in reciprocal space for $t = 520$ nm. We define the topological charge as the winding number of the polarization vector (c_x, c_y) around a BIC in reciprocal space as in Ref. [40]. Here, c_x and c_y are the coefficients of far-field radiation with electric fields along the x and y directions, respectively. The vortex (antivortex) exhibits a positive (negative) topological charge. By decreasing t , these two BICs with opposite charges gradually approach each other and finally collide at $t = 513.7$ nm [the right panel of Fig. 2(e)]. This corresponds to the merging BIC case, and the Q factor along the ΓM direction is given by the solid cyan line in Fig. 2(d). The Q factor remains sufficiently large over a broad wave vector range around the Q diverging point, which shows the typical feature of a merging BIC. By further decreasing t , these two BICs annihilate each other and form a quasi-BIC with a high but not divergent Q factor [magenta solid line in Fig. 2(d) for $t = 512$ nm].

The two BIC tracks in Fig. 2(c) exhibit the typical feature of “anticrossing” (see the red and blue dashed lines for eye guidance). The red dashed line approximately follows the evolution of the anticrossing point [the white dashed line in Fig. 2(c)], thus fitting the description of the FW-BIC. The other BIC here is an accidental BIC similar to that described in Refs. [12,40,61]. Considering a larger range of t , we can see the approach of another accidental BIC, while the FW-BIC still approximately follows the anticrossing point (Supplemental Material [57], Sec. III). Moreover, the FW-BIC exhibits the same scaling rule as $Q \sim (k - k_{\text{BIC}})^{-2}$ with the accidental BIC [44] in the vicinity of the BICs (Supplemental Material [57], Sec. IV). Figure 2(f) shows the fitting of the Q factor, wherein Q geometrically decays as $Q \sim (k - k_{\text{BIC}})^{-2}$ for both the accidental BIC (blue) and the FW-BIC (red). When these two isolated BICs merge, Q decays as $(k - k_{\text{BIC}})^{-4}$ (green), much lower than the two isolated BICs (Supplemental Material [57], Sec. IV). Moreover, the nearby Q of the merging BIC case is orders of magnitude higher than both the FW-BIC and the accidental

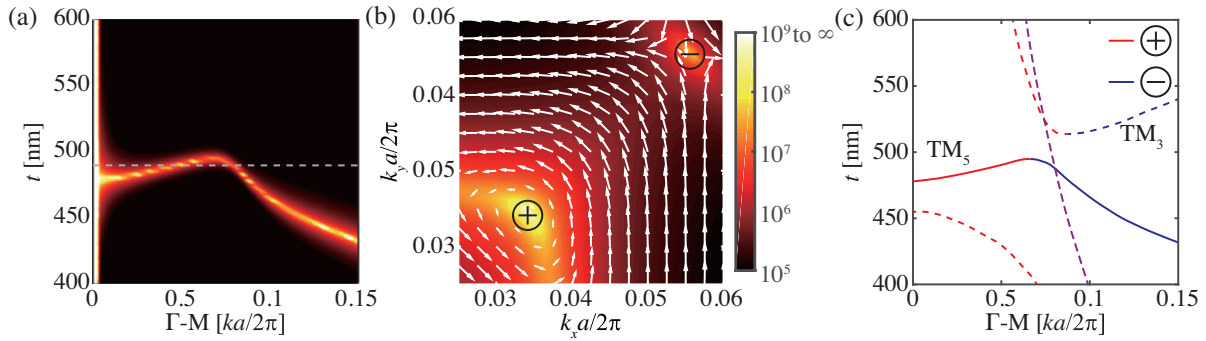


FIG. 3. (a) The simulated evolution of the Q factor along ΓM for the TM_5 band. The dashed line marks $t = 490$ nm. (b) Calculated polarization vectors with the Q factor as the background for the BIC pair at $t = 490$ nm. (c) Charge trajectories of the BIC pair on the TM_3 band (dashed) and TM_5 band (solid). The dashed magenta line shows the trajectory of the anticrossing point.

BIC, which can lead to much better performance in applications [44].

The red, cyan, and magenta dashed lines in Fig. 2(d) show the Q factor of the TM_5 band along the ΓM direction for $t = 520, 513.7,$ and 512 nm, respectively. In addition to the well-known symmetry-protected BIC at Γ [9,11], there are no other BICs. Intriguingly, another merging BIC emerges on the TM_5 band as we further decrease t . Figure 3(a) shows the Q factor of the TM_5 band along the ΓM direction as we vary t , wherein we can identify BICs traced by a high Q factor curve. The polarization vectors together with the Q factor for $t = 490$ nm are shown in Fig. 3(b). Here, the high Q points also correspond to the center of the vortex or antivortex, and hence indicate that they are indeed BICs. Figure 3(c) shows the charge trajectories for the TM_5 band (solid line) together with the TM_3 band (dashed lines) as a reference, wherein red (blue) represents the positive (negative) topological charge. With decreasing of t , after the merging BIC on the TM_3 band evolves into a quasi-BIC, another quasi-BIC then gradually evolves into a merging BIC on the TM_5 band near the anticrossing point (magenta dashed line). As we further decrease t , the merging BIC on the TM_5 band decomposes into two isolated BICs with opposite charges.

Merging BIC at an arbitrary location.—Previously, we have preserved C_{4v} symmetry which simplifies the search for BICs that are forced to locate in the ΓM and ΓX directions. Actually, the isolated BICs and the merging BICs can be tuned to almost arbitrary \mathbf{k} points when the proper symmetries are broken. The definition of topological charge requires the polarization vectors (c_x, c_y) to be real, which are protected by $C_2^z T$ (C_2^z : 180° rotation symmetry around the z axis, T : time-reversal symmetry) [40]. Thus, the isolated BICs are topologically robust when the PCS possesses both $C_2^z T$ and σ_h symmetry. Here, we also maintain σ_h symmetry to ensure that the $+z$ and $-z$ radiation channels are the same [37]. Figure 4(a) shows the unit cell where $C_2^z T$ symmetry is preserved while in-plane mirror symmetries are all broken. Here, the circular hole on

the Si_3N_4 PCS is replaced by an elliptical hole with the short axis rotated by θ . The band structure of this PCS is similar to that in Fig. 2(b) (Supplemental Material [57], Sec. IX); here, we still focus on the TM_3 band. The polarization vectors together with the Q factor are shown in Fig. 4(b) for $t = 516$ nm. A vortex (charge $+1$) and an antivortex (charge -1) are clearly tuned away from the ΓM direction. Figure 4(c) shows the polarization vectors together with the Q factor for $t = 512$ nm, where two isolated BICs merge at $(0.127\pi/a, 0.087\pi/a)$. We emphasize that these two isolated BICs merge by varying only t ,

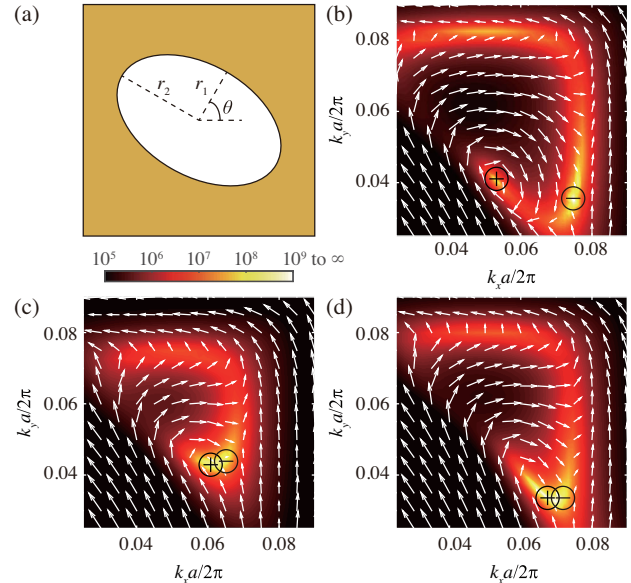


FIG. 4. (a) Diagram of the unit cell with elliptical holes, where yellow represents Si_3N_4 and white represents $n = 1.45$. The calculated distribution of polarization vectors with the Q factor as background for (b) BIC pair with $\theta = 60^\circ$, $t = 516$ nm, (c) merging BIC at $(0.127\pi/a, 0.087\pi/a)$ with $\theta = 60^\circ$, $t = 512$ nm, and (d) merging BIC at $(0.14\pi/a, 0.065\pi/a)$ with $\theta = 75^\circ$, $t = 514$ nm. In (b)–(d), the lattice constant, short axis, and long axis are kept at $a = 334$, $r_1 = 80$, and $r_2 = 128$ nm, respectively.

as we have already fine-tuned the other parameters. In principle, two independent parameters are needed to form a merging BIC. The merging BICs can also be tuned to other k points. The merging BIC appears at $(0.14\pi/a, 0.065\pi/a)$ in Fig. 4(d) with $\theta = 75^\circ$, $t = 514$ nm while the other parameters remain unchanged. Moreover, the change from a circular hole to an elliptical hole enables us to merge BICs at a fixed thickness, which favors the commercially available PCSs (Supplemental Material [57], Sec. V).

Summary.—In conclusion, we have demonstrated a feasible approach to construct merging BICs at almost arbitrary points in reciprocal space. We start with a PCS that supports the concurrence of an FW-BIC and an accidental BIC. $C_2^z T$ symmetry ensures that these two BICs exhibit topological charges and hence can be continuously moved in reciprocal space. By varying the thickness of the PCS, these two BICs carrying opposite charges merge to form a merging BIC, which exhibits all nearby Q factors far higher than the previous two. By keeping $C_2^z T$ and σ_h symmetries while breaking all other in-plane mirror symmetries, the merging BIC can be tuned to almost an arbitrary position in reciprocal space. If we further break the C_2^z symmetry, the FW-BIC and accidental BIC break into pairs of half vortices with circularly polarized states having opposite handedness as topological defects (Supplemental Material [57], Sec. VI). Since the FW-BIC and accidental BICs are quite common on the band structure, our approach is general and flexible. Merging BICs with a robust (Supplemental Material [57], Sec. VII), superhigh Q factor enrich the exploration of topological photonics and are potentially useful for nonlinear and quantum effects, large-area lasers and the improvement of optoelectronic devices. Furthermore, off- Γ merging BICs have designable momentum and wavelength, and thus have potential applications in on-chip beam steering, directional vector beams, diffraction-free beams, directivity modulators, narrowband filters (Supplemental Material [57], Sec. VIII), and chemical or biological sensing based on the ultrasensitive angular selectivity (Supplemental Material [57], Sec. VIII).

This work is supported by the National Natural Science Foundation of China (Grants No. 91850207, No. 11904264, No. 11674255, and No. 11674256), the National Key R&D Program of China (Grants No. 2017YFA0303504 and No. 2017YFA0205800), and the Strategic Priority Research Program of Chinese Academy of Sciences (Grant No. XDB30000000). M. X. is also supported by the startup funding of Wuhan University.

* spzhang@whu.edu.cn

† phmxiao@whu.edu.cn

‡ hxxu@whu.edu.cn

- [1] C. W. Hsu, B. Zhen, A. D. Stone, J. D. Joannopoulos, and M. Soljačić, *Nat. Rev. Mater.* **1**, 16048 (2016).
- [2] J. von Neumann and E. Wigner, *Phys. Z.* **30**, 465 (1929).
- [3] H. Friedrich and D. Wintgen, *Phys. Rev. A* **32**, 3231 (1985).
- [4] M. I. Molina, A. E. Miroshnichenko, and Y. S. Kivshar, *Phys. Rev. Lett.* **108**, 070401 (2012).
- [5] G. Corielli, G. Della Valle, A. Crespi, R. Osellame, and S. Longhi, *Phys. Rev. Lett.* **111**, 220403 (2013).
- [6] P. J. Cobelli, V. Pagneux, A. Maurel, and P. Petitjeans, *Europhys. Lett.* **88**, 20006 (2009).
- [7] Y. X. Xiao, G. Ma, Z. Q. Zhang, and C. T. Chan, *Phys. Rev. Lett.* **118**, 166803 (2017).
- [8] D. C. Marinica, A. G. Borisov, and S. V. Shabanov, *Phys. Rev. Lett.* **100**, 183902 (2008).
- [9] S. Fan and J. D. Joannopoulos, *Phys. Rev. B* **65**, 235112 (2002).
- [10] Y. Plotnik, O. Peleg, F. Dreisow, M. Heinrich, S. Nolte, A. Szameit, and M. Segev, *Phys. Rev. Lett.* **107**, 183901 (2011).
- [11] J. Lee, B. Zhen, S. L. Chua, W. Qiu, J. D. Joannopoulos, M. Soljačić, and O. Shapira, *Phys. Rev. Lett.* **109**, 067401 (2012).
- [12] C. W. Hsu, B. Zhen, J. Lee, S. L. Chua, S. G. Johnson, J. D. Joannopoulos, and M. Soljačić, *Nature (London)* **499**, 188 (2013).
- [13] S. Weimann, Y. Xu, R. Keil, A. E. Miroshnichenko, A. Tünnermann, S. Nolte, A. A. Sukhorukov, A. Szameit, and Y. S. Kivshar, *Phys. Rev. Lett.* **111**, 240403 (2013).
- [14] F. Monticone and A. Alù, *Phys. Rev. Lett.* **112**, 213903 (2014).
- [15] E. N. Bulgakov and D. N. Maksimov, *Phys. Rev. Lett.* **118**, 267401 (2017).
- [16] M. V. Rybin, K. L. Koshelev, Z. F. Sadrieva, K. B. Samusev, A. A. Bogdanov, M. F. Limonov, and Y. S. Kivshar, *Phys. Rev. Lett.* **119**, 243901 (2017).
- [17] J. Gomis-Bresco, D. Artigas, and L. Torner, *Nat. Photonics* **11**, 232 (2017).
- [18] S. I. Azzam, V. M. Shalaev, A. Boltasseva, and A. V. Kildishev, *Phys. Rev. Lett.* **121**, 253901 (2018).
- [19] M. Minkov, I. A. D. Williamson, M. Xiao, and S. Fan, *Phys. Rev. Lett.* **121**, 263901 (2018).
- [20] A. Cerjan, C. W. Hsu, and M. C. Rechtsman, *Phys. Rev. Lett.* **123**, 023902 (2019).
- [21] R. Mermet-Lyauoz, F. Dubois, N.-V. Hoang, E. Drouard, L. Berguiga, C. Seassal, X. Letartre, P. Viktorovitch, and H. S. Nguyen, *arXiv:1905.03868*.
- [22] W. Ye, Y. Gao, and J. Liu, *Phys. Rev. Lett.* **124**, 153904 (2020).
- [23] T. Yoda and M. Notomi, *Phys. Rev. Lett.* **125**, 053902 (2020).
- [24] Q. Song, J. Hu, S. Dai, C. Zheng, D. Han, J. Zi, Z. Q. Zhang, and C. T. Chan, *Sci. Adv.* **6**, eabc1160 (2020).
- [25] A. Kodigala, T. Lepetit, Q. Gu, B. Bahari, Y. Fainman, and B. Kanté, *Nature (London)* **541**, 196 (2017).
- [26] V. Mylnikov, S. T. Ha, Z. Pan, V. Valuckas, R. Paniagua-Dominguez, H. V. Demir, and A. I. Kuznetsov, *ACS Nano* **14**, 7338 (2020).
- [27] Z. Liu, Y. Xu, Y. Lin, J. Xiang, T. Feng, Q. Cao, J. Li, S. Lan, and J. Liu, *Phys. Rev. Lett.* **123**, 253901 (2019).
- [28] M. Minkov, D. Gerace, and S. Fan, *Optica* **6**, 1039 (2019).

- [29] K. Koshelev, S. Kruk, E. Melik-Gaykazyan, J. H. Choi, A. Bogdanov, H. G. Park, and Y. Kivshar, *Science* **367**, 288 (2020).
- [30] V. Kravtsov *et al.*, *Light Sci. Appl.* **9**, 56 (2020).
- [31] F. Yesilkoy, E. R. Arvelo, Y. Jahani, M. Liu, A. Tittl, V. Cevher, Y. Kivshar, and H. Altug, *Nat. Photonics* **13**, 390 (2019).
- [32] Y. Guo, M. Xiao, Y. Zhou, and S. Fan, *Adv. Opt. Mater.* **7**, 1801453 (2019).
- [33] W. Liu, B. Wang, Y. Zhang, J. Wang, M. Zhao, F. Guan, X. Liu, L. Shi, and J. Zi, *Phys. Rev. Lett.* **123**, 116104 (2019).
- [34] B. Bahari, F. Vallini, T. Lepetit, R. Tellez-Limon, J. H. Park, A. Kodigala, Y. Fainman, and B. Kante, *arXiv:1707.00181*.
- [35] B. Wang, W. Liu, M. Zhao, J. Wang, Y. Zhang, A. Chen, F. Guan, X. Liu, L. Shi, and J. Zi, *Nat. Photonics* **14**, 623 (2020).
- [36] C. Huang *et al.*, *Science* **367**, 1018 (2020).
- [37] X. Yin, J. Jin, M. Soljacic, C. Peng, and B. Zhen, *Nature (London)* **580**, 467 (2020).
- [38] S. I. Azzam and A. V. Kildishev, *Adv. Opt. Mater.* **9**, 2001469 (2021).
- [39] K. Sakoda, *Optical Properties of Photonic Crystals* (Springer Science & Business Media, Berlin, 2004).
- [40] B. Zhen, C. W. Hsu, L. Lu, A. D. Stone, and M. Soljacic, *Phys. Rev. Lett.* **113**, 257401 (2014).
- [41] H. M. Doeleman, F. Monticone, W. den Hollander, A. Alù, and A. F. Koenderink, *Nat. Photonics* **12**, 397 (2018).
- [42] Y. Zhang, A. Chen, W. Liu, C. W. Hsu, B. Wang, F. Guan, X. Liu, L. Shi, L. Lu, and J. Zi, *Phys. Rev. Lett.* **120**, 186103 (2018).
- [43] W. Chen, Y. Chen, and W. Liu, *Phys. Rev. Lett.* **122**, 153907 (2019).
- [44] J. Jin, X. Yin, L. Ni, M. Soljacic, B. Zhen, and C. Peng, *Nature (London)* **574**, 501 (2019).
- [45] Y. Kurosaka, S. Iwahashi, Y. Liang, K. Sakai, E. Miyai, W. Kunishi, D. Ohnishi, and S. Noda, *Nat. Photonics* **4**, 447 (2010).
- [46] M. Imada, A. Chutinan, S. Noda, and M. Mochizuki, *Phys. Rev. B* **65**, 195306 (2002).
- [47] S. T. Ha, Y. H. Fu, N. K. Emani, Z. Pan, R. M. Bakker, R. Paniagua-Dominguez, and A. I. Kuznetsov, *Nat. Nanotechnol.* **13**, 1042 (2018).
- [48] S. I. Azzam, K. Chaudhuri, A. Lagutchev, Z. Jacob, Y. L. Kim, V. M. Shalaev, A. Boltasseva, and A. V. Kildishev, *arXiv:2006.16473*.
- [49] Y. Lin, T. Feng, S. Lan, J. Liu, and Y. Xu, *Phys. Rev. Applied* **13**, 064032 (2020).
- [50] C.-L. Zou, J.-M. Cui, F.-W. Sun, X. Xiong, X.-B. Zou, Z.-F. Han, and G.-C. Guo, *Laser Photonics Rev.* **9**, 114 (2015).
- [51] X. W. Gao, B. Zhen, M. Soljacic, H. S. Chen, and C. W. Hsu, *ACS Photonics* **6**, 2996 (2019).
- [52] L. L. Doskolovich, E. A. Bezus, and D. A. Bykov, *Photonics Res.* **7**, 1314 (2019).
- [53] Z. Yu and X. Sun, *Light Sci. Appl.* **9**, 1 (2020).
- [54] A. Leitis, A. Tittl, M. Liu, B. H. Lee, M. B. Gu, Y. S. Kivshar, and H. Altug, *Sci. Adv.* **5**, eaaw2871 (2019).
- [55] M. Rybin and Y. Kivshar, *Nature (London)* **541**, 164 (2017).
- [56] W. Suh, Z. Wang, and S. Fan, *IEEE J. Quantum Electron.* **40**, 1511 (2004).
- [57] See Supplemental Material at <http://link.aps.org/supplemental/10.1103/PhysRevLett.126.117402> for details, including I. numerical simulation method, II. temporal coupled-mode theory model, III. topological charge evolution, IV. scaling rule of FW-BIC and merging BICs, V. parameter tuning with the aspect ratio of an elliptical hole, VI. circular polarization spawning from BICs, VII. robustness of merging BICs against fabrication imperfections, VIII. reflection spectra near merging BICs and refractive index sensing, and IX. supplemental figures. The Supplemental Material includes Refs. [58].
- [58] V. Liu and S. Fan, *Comput. Phys. Commun.* **183**, 2233 (2012).
- [59] A. Volya and V. Zelevinsky, *Phys. Rep. C* **67**, 054322 (2003).
- [60] COMSOL Multiphysics® v. 5.2a. www.comsol.com. COMSOL AB, Stockholm, Sweden.
- [61] Y. Yang, C. Peng, Y. Liang, Z. Li, and S. Noda, *Phys. Rev. Lett.* **113**, 037401 (2014).